

Experimental and Numerical Study of Spar Buoy-magnet/spring Oscillators Used as Wave Energy Absorbers

Annette R. Grilli¹, Jon Merrill¹, Stéphan T. Grilli¹, Malcolm L. Spaulding¹, and Jeffrey T. Cheung²

1. Department of Ocean Engineering, University of Rhode Island, Narragansett, RI, USA

2. Teledyne Scientific and Imaging, Thousand Oaks, CA, USA

ABSTRACT

We study free-floating point absorption wave generators, consisting of an assemblage of one or a few (mostly heaving) spar buoys, housing at least one short-stroke linear generator (SSLG), made of a magnet, suspended to a spring, and oscillating within a coil. This system is aimed at producing low and renewable wave power (up to $\mathcal{O}(1)$ kW) for marine coastal surveillance systems. Both scale model experiments and numerical modeling are performed in order to tune the system's parameters and maximize its response for a target sea-state (i.e., operate near resonance in heave and magnet motion). We find that, for such buoy systems, viscous friction is the dominant damping mechanism near resonance and, hence, the buoy's wet extremities must also be properly streamlined, and rolling must be minimized as it may significantly increase such damping. This can be achieved with a so-called *trispars* system, in which 3 spars buoys of identical diameter are mounted in an equilateral triangle configuration, one diameter apart from each other. Since the heave resonance period of a spar buoy is primarily a function of its draft, to lower this period and better match the resonance period of the SSLG, the draft of each buoy in the trispars is varied (in the scale model, to 25, 50 and 100 cm), with the longest spar buoy housing the SSLG, while simultaneously adjusting their dead weight.

Experimental results in periodic waves, well supported by numerical modeling, show a significantly improved performance of the trispars vs. single spar design, both with respect to parasitic roll oscillations (almost none observed for the tripar) and power generation. The good performance of the trispars, particularly in terms of "Capture Width Ratio", is confirmed by preliminary numerical simulations in irregular waves. Future work will test the trispars in irregular waves and explore dynamic tuning strategies (e.g., latching) of the SSLG, in order to further improve power generation.

KEYWORDS : Wave energy systems; heaving buoy; linear energy generator; floating body dynamic; Boundary Integral Equations; linear waves.

INTRODUCTION

Our goal is to develop a system to produce low amounts of power ($\mathcal{O}(1)$ kW) for marine surveillance instrumentation (e.g., autonomous target recognition instruments, persistence and ubiquitous sensor systems, tracking and identification of maritime vessels, and miniature underwater sensor networks), based on capturing renewable wave energy. To do so, we design and optimize a new type of freely floating, slackly moored buoy, housing a "Short Stroke Linear Generator" (SSLG), made of spring, magnet, and coil components. The response to periodic and irregular wave forcing, of the double oscillator constituting the buoy-SSLG system, is analyzed using both state-of-the-art numerical models and scale model testing in a laboratory wave tank.

Our system falls within the general category of independent oscillators, point absorbers (Stallard et al, 2005). [A review of various forms of ocean wave energy systems can be found in, e.g., Previsic et al (2004).] The key features inherent in this type of design include response to omni-directional wave forcing, direct conversion from mechanical energy of the buoy motion to electrical energy, thus eliminating the need for an intermediate component in the power take off system (e.g. turbine), no external working parts, and minimizing the number of moving parts and complexity of the structure and system. Budal and Falnes (1975), French (1979), and French and Bracewell (1995), have concluded that the most promising and economical form of these types of systems are those that can be tuned to the frequency of the waves present in the ocean and hence take advantage of the increased amplitude of motion at the natural heave frequency of the system. Given the low power applications that are targeted, the desire

to have the physical size of the system limited so that it can be routinely deployed and retrieved from either a surface vessel or even helicopter, and to keep the construction and maintenance costs as low as possible, a simple spar buoy design (both single- and multiple-spars) was pursued.

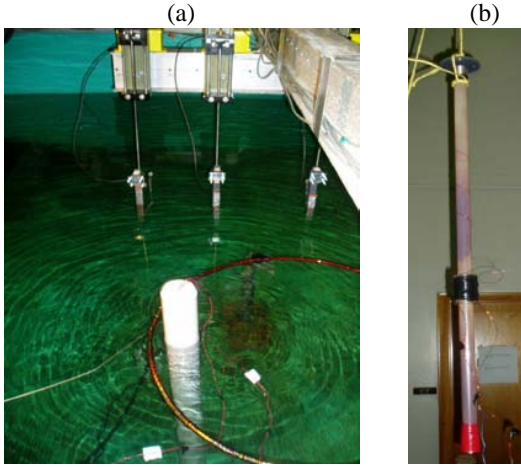


Fig. 1 : (a) Spar buoy model SB3 in wave tank ($D = 0.09$ m, $d = 1$ m), forced by $A = 1.5$ cm and $T = 1.5$ s waves. Capacitance wave gauges, buoy containment rink, and SSLG output wires are shown. (b) SSLG undergoing dry testing.

Three major, linked subsystems, are considered in the design: (i) *buoy dynamics*, i.e., mechanical buoy response to wave forcing; (ii) *generator mechanical dynamics*, i.e., response of the SSLG resulting from the movements of the buoy (motion of magnet relative to the coils); and (iii) *generator electric dynamics*, i.e., determining the electrical power output from the linear generator, given the dynamics of the armature-stator system. In the most general case, there are feedbacks between the various components of the system, that must be considered to optimize its overall performance. As an example, the movement of the armature will result in a change of the weight distribution and hence impact the buoys movement. Similarly the electro-magnetic force from the armature-stator system will alter the mechanical response of the generator. In the present study, the focus has been restricted to the buoy and mechanical SSLG dynamics portion of the problem (systems (i) and (ii)). In the experimental part of this work, the heaving buoy(s) are equipped with a SSLG model, built by Teledyne Scientific and Imaging, LLC (TSI), in which a new type of friction reduction *ferrofluid* is used, as a fluid cushion between the moving magnet and the coil. Hence, magnet damping due to friction becomes negligible as compared to mechanical damping due to electro-magnetic interactions between the magnet and the coil.

Power production can be maximized by tuning the response of subsystems (i) and (ii) to wave forcing. The goal is to select parameters so that the mechanical responses of the buoy and the SSLG are near resonance for the most prevalent wave conditions. Ideally, in accordance with typical ocean wave energy spectra, the system should have broadband response so that it optimizes wave energy capture over a range of wave frequencies, and not just at

one fixed frequency. Systems can be tuned to improve their response by fixed, slow, and fast tuning. Fixed tuning refers to properties of the device (size, shape, and mass), that are established in the basic design and hence not readily changed once the buoy is constructed and deployed. Slow tuning refers to changes in the response on time scales of minutes to hours and typically is focused on changing the systems buoyancy and hence its mass and effective stiffness. This can be achieved by active ballast control. Fast tuning actively controls system dynamics on time scales of variations of individual waves or wave groups. The latter tuning is typically very difficult to implement because device characteristics must be changed quickly enough to alter its response. Also, for typical irregular sea states, one cannot exactly predict waves that are about to reach the system (and thus dynamically tune it for such waves), and hence one can only make a forecast and iteratively correct it over a number of wave periods (e.g., Babarit and Clément, 2006). In this initial work, we only explore fixed tuning of the system.

THE ANALYTICAL AND NUMERICAL MODELS

Dynamic of the heaving spar buoy

We consider a rigid spar buoy of cylindrical shape, with draft d , external diameter D , and length ℓ (Fig. 1a), floating in water of specific mass ρ and depth h . The submerged extremity of the buoy is streamlined to reduce friction drag generated during motion, but this slight change of geometry is neglected in the following idealized analysis. For slender spar buoys, the heave natural frequency can be predicted by the simplified equation, $\omega_{H0} = \sqrt{g/d}$ (Berteaux, 1994). Using the numerical model detailed below, we verified that this equation is accurate for $D/d < 0.1$.

In transient waves, the buoy heaving motion in the time domain, denoted here by $y(t)$, under the action of inertia, radiative wave damping, viscous damping, gravity, and buoyancy forces, is governed by the 2nd-order nonlinear Ordinary Differential Equation (ODE),

$$(M + a_{33}(\infty)) \ddot{y} + \int_0^t \mathcal{K}(t - \tau) \dot{y}(\tau) d\tau + b | \dot{y} - w | (\dot{y} - w) + c_{33} y = F_3(t) [+K_s z] \quad (1)$$

where the upper dots denote time derivatives, $M = \rho \forall$ is the buoy mass (with $\forall = S_o d$, the buoy displacement), $a_{33}(\infty)$ the instantaneous heave added mass (i.e., for a very large frequency),

$$b = \frac{1}{2} \rho S_o C_d \quad (2)$$

is the viscous damping coefficient, with C_d the drag coefficient and $S_o = \pi D^2/4$ the horizontal buoy cross-section, $c_{33} = \rho g S_o$ is the buoyancy restoring term, w is the wave vertical particle velocity (defined later), and $F_3(t)$ is the heave wave excitation force. The bracketed term in the right-hand-side is a feedback coupling force due to the spring/magnet oscillator motion, which will be discussed later.

The integral in Eq. (1) represents a memory term (e.g., Babarit et al., 2006), in which $\mathcal{K}(t)$, the heave impulse response function, can be calculated as a function of the buoy frequency response by either of the inverse Fourier transforms (Lee, 1995),

$$\begin{aligned}\mathcal{K}(t) &= \frac{2}{\pi} \int_0^\infty (a_{33}(\omega) - a_{33}(\infty)) \cos \omega t \, d\omega \\ \mathcal{K}(t) &= \frac{2}{\pi} \int_0^\infty b_{33}(\omega) \sin \omega t \, d\omega\end{aligned}\quad (3)$$

as a function of $a_{33}(\omega)$ and $b_{33}(\omega)$, the frequency dependent heave added mass and wave radiative damping terms, respectively.

Assuming superposition of linear periodic waves, for any given sea-state represented by a wave energy density spectrum $S(\omega)$ (e.g., Pierson-Moskowitz (PM) or JONSWAP (JS)), the time dependent free surface elevation can be expressed as,

$$\eta(t) = \sum_{n=1}^N A_n \cos(\omega_n t + \psi_n) \quad (4)$$

where, for a specified set of random phases $\psi_n \in [0, 2\pi]$, the amplitude A_n of each harmonic wave component of frequency ω_n can be obtained by inverse Fourier transform of the spectrum. Accordingly, the wave heave excitation force can be calculated as,

$$F_3(t) = \rho g \sum_{n=1}^N A_n r_{3n} \cos(\omega_n t + \phi_{3n} + \psi_n) \quad (5)$$

where, for each of N wave components, $(r_{3n}(\omega_n), \phi_{3n}(\omega_n))$ are the module and phase, respectively of the heave exciting force caused on the buoy by a periodic wave of unit amplitude and frequency ω_n (including diffraction effects).

The frequency dependent coefficients $(a_{33}, b_{33}, r_3, \phi_3)$, in the above equations, are calculated using the standard Boundary Element code WAMIT (Lee, 1995; Newman, 1977), in which linear free surface boundary conditions are assumed. Specifically, once specified the buoy geometry and mass distribution, computations are performed with WAMIT, for N equally spaced periods T_n (with $\omega_n = 2\pi/T_n$), in the specified interval (T_{min}, T_{max}) . WAMIT's procedure F2T can also provide $\mathcal{K}(t)$, by calculating the integrals in Eq. (3), if required.

As we shall see, for slender spar buoys with $D/d < 0.1$, a_{33} is small and varies very little over any useful frequency interval including the buoy heave resonance frequency ω_{H0} , while b_{33} is very small, reflecting the fact that such buoys generate very little waves in heaving motion. Thus, Eqs. (3) yields $\mathcal{K}(t) \simeq 0$, and hence the memory term in Eq. (1) is negligible, particularly as compared to the viscous damping term. Accordingly, the ODE governing the transient heaving motion of a slender spar buoy can be simplified to,

$$M'_{33} \ddot{y} + b_{33p} \dot{y} + b |\dot{y} - w|(\dot{y} - w) + c_{33} y = F_3 [+K_s z] \quad (6)$$

with $M'_{33} = M + a_{33p}$, (a_{33p}, b_{33p}) the heave added mass and radiative damping at the dominant frequency of the sea state, respectively (typically, the peak spectral frequency ω_p), and $F_{33}(t)$

given by Eq. (5). [Note, the second term is kept in Eq. (6) to have the same damping outside of the resonant frequency band, where viscous damping vanishes, as in the linear periodic case detailed below.] For linear periodic waves, we also have,

$$w(t) = \sum_{n=1}^N A_n \omega_n \frac{\sinh k_n (h-d)}{\sinh k_n h} \sin(\omega_n t + \psi_n) \quad (7)$$

with the wavenumber k_n given, for each wave component, by the linear dispersion relationship,

$$\omega_n^2 = g k_n \tanh(k_n h) \quad (8)$$

which simplifies to $k_n \simeq \omega_n^2/g$ for deep water waves ($k_n h > \pi$). Eqs. (5) to (8) are implemented as a MATLAB program that directly reads WAMIT outputs. After being transformed into a system of two 1st-order ODEs by change of variables, the nonlinear 2nd-order ODE (6) is time integrated by a Runge-Kutta method, using a standard MATLAB function. Initial conditions are simply set to $y = \dot{y} = 0$ for $t = 0$. Computations are usually pursued up to at least $t = 150 T_p$, with $T_p = 2\pi/\omega_p$ the peak spectral period. If the buoy is subjected to periodic waves only, the same WAMIT-MATLAB (WM) model is applied, from an initial state of rest, assuming $N = 1$, until the transient buoy motion reaches a periodic state.

In the periodic case, linearized equations governing the buoy motion for 6 degrees of freedom (dof) can be expressed in complex form (e.g., Newman, 1977); for the heave dof, we have,

$$\{-\omega^2(M + a_{33}) + i\omega b_{33} + c_{33}\} \xi_3 = A r_3 e^{i\psi_3} \quad (9)$$

with $M = M_{33}$, $i = \sqrt{-1}$, a wave of amplitude A and frequency ω , and ξ_3 the complex amplitude of the buoy heave motion. A frequency dependent Response Amplitude Operator (RAO) can be defined for each dof; for heave: $Z_3 = |\xi_3|/A$. Solving Eq. (9) yields, for a spar buoy in simple heaving motion,

$$Z_3 = r_3(\omega) \left\{ \{c_{33} - \omega^2(M + a_{33}(\omega))\}^2 + \omega^2 b_{33}^2 \right\}^{-\frac{1}{2}} \quad (10)$$

Maximum heave response $Z_3^{max} = r_3/(\omega b_{33})$ occurs if,

$$\omega = \sqrt{\frac{c_{33}}{M + a_{33}(\omega)}} = \omega_H \quad (11)$$

With $a_{33} \ll M$ for a slender spar buoy, Eq. (11) yields $\omega_H \simeq \omega_{H0}$, the heave natural frequency defined above. In the absence of viscous damping and with a very small value for b_{33} , it can be shown that the maximum heave response predicted near the resonance frequency using Eq. (10) (such as done in WAMIT), is overestimated by a factor of 10-20 in most cases, as compared to laboratory measurements. When solving Eqs. (6) to (8), and properly calibrating the drag coefficient C_d , however, predictions of the WM model agree very well with measurements, even near the natural resonance frequency.

Dynamic of the spring-magnet oscillator

Similar to the spar buoy, a 2nd-order linear ODE is derived to describe the motion of the spring-magnet system, denoted by $z(t)$, that is at the core of the SSLG. Assuming a magnet suspended by a single spring, this equation has mass, linear damping, and spring restoring terms in the left-hand-side, and is forced in the right hand side by the inertia force induced on the spring-magnet system by the buoy heaving motion,

$$M_s \ddot{z} + \mu \dot{z} + K_s z = M_s \ddot{y} \quad (12)$$

with M_s the spring-magnet mass, μ the damping coefficient and K_s the spring stiffness. If the magnet is suspended in between two springs of stiffnesses K_1 and K_2 , we simply have $K_s = K_1 + K_2$. If, at static equilibrium of the SSLG, the springs have initial lengths l_1 and l_2 from their non-deformed state, we have,

$$M_s g = K_2 l_2 - K_1 l_1 \quad (13)$$

when spring 2 is located above spring 1. If only spring 2 is used, we find $l_s = M_s g / K_s$ for the initial (static) extension of the spring.

Solving Eq. (12), with $z = 0 = \dot{z} = 0$ at $t = 0$, for a harmonic forcing of amplitude $M_s a_o A$ and frequency ω on the right-hand-side, we find the spring-magnet RAO $R = |z|/A$ as,

$$R = M_s a_o \left\{ \{K_s - \omega^2 M_s\}^2 + \omega^2 \mu^2 \right\}^{-\frac{1}{2}} \quad (14)$$

As for the buoy, we find that maximum response $R^{max} = M_s a_o / (\omega \mu)$ occurs at the natural frequency of the system,

$$\omega = \sqrt{\frac{K_s}{M_s}} = \sqrt{\frac{g}{l_s}} = \omega_s \quad (15)$$

which, for a single spring, only depends on the spring static extension; in particular, the longer the SSLG, the lower its natural frequency. In practice, having $\omega_s = \omega_{H0}$ requires $l_s \simeq d$, and having these frequencies matching the peak spectral wave frequency ω_p , while keeping the spar buoy within a reasonable size, may be difficult, particularly considering that, due to magnet motion, the total length of the SSLG that must fit within the buoy length ℓ is typically closer to $2l_s$. For instance, for $T_p = 8$ s (corresponding to a typical swell peak), we find $d = l_s = 15.9$ m, which makes the buoy prohibitively long. For typical shelf wave conditions in New England, however, we have $T_p \simeq 4.5$ s, which yields $d = l_s \simeq 5$ m, which may be achievable with a buoy of, say, total length $\ell = 7$ m or so.

After transforming Eq. (12) in a system of two 1st-order ODEs by change of variables, the system of 4 first-order ODEs resulting from Eqs. (6) and (12) is time integrated, using the standard MATLAB function mentioned before, to simultaneously provide $y(t)$ and $z(t)$. In this coupled ODE system, due to its motion, the SSLG creates a feedback reaction force onto the buoy casing, that is represented by a $K_s z$ force in the right-hand-side

of Eqs. (1) and (6) (the bracketed term). This force is quite small for typical spring constants used in the SSLG, as compared to the other forces in the equation. However, its effect on the buoy dynamics may become significant for large amplitude motions near resonance, as we shall see in the application section below.

Finally, one can calculate the mechanical power extracted from the magnet motion, corresponding to the magnet damping force $\mu \dot{z}$ in Eq. (12), as $P_\mu(t) = \mu \dot{z}^2$. Coefficient μ , which here is a specified parameter, should in fact be derived from the *emf* force generated between the coil, built around the generator, and the magnet, due to their electro-magnetic interactions, as a function of the magnet strength and coil circuit characteristics. This electro-magnetic part was not modeled in this work and, in the applications, the damping coefficient is simply adjusted in order to yield P_μ values in agreement with those measured in wavetank tests of the generator. We further define $\mu = \mu' M_s \omega_s$ and use the non-dimensional coefficient μ' in applications.

APPLICATIONS

Laboratory experiments and numerical simulations are performed to design a spar buoy-based system, equipped with a SSLG, to capture renewable wave energy. The prototype system performance is to be optimized for shelf wave conditions, i.e., $T_p \simeq 4.5$ s. For a single spar buoy, assuming $T_{H0} = T_p$, this leads to a prototype draft of $d = 5$ m and, to satisfy the slender spar buoy requirement, a buoy exterior diameter $D < 0.5$ m. Scale model experiments were performed in the wavetank of the University of Rhode Island, Department of Ocean Engineering (30 m long, 1.8 m deep and 3.6 m wide), which is equipped with a flap wavemaker operating in the periods range $T \in [0.5, 2.5]$ s. Periodic waves, with amplitude $A \in [0.015, 0.06]$ m were generated in water of depth $h = 1.3$ m. Based on linear theory, this created deep water waves for $T \leq 1.3$ s and intermediate water depth waves for $1.3 < T \leq 3$ s.

A geometric scale of $\alpha = 1/10$ was selected and a series of cylindrical spar buoy models were initially built and tested, with draft $d = 0.5$ m, length $\ell = 0.6$ to 0.7 m, and diameter $D \simeq 0.04$ or 0.06 m (e.g., Fig. 1a). To reduce the viscous drag coefficient C_d and maximize heaving motion, each buoy submerged end was equipped with a streamlined nose cap. These initial buoy models were constructed without a SSLG installed within them, but they had an equivalent distribution of mass and, hence, location of the center of mass, as the planned prototype. Subsequent buoy models were built and tested with an internal SSLG (Figs. 1a,b). All models were equipped with high precision, remotely operated, three-axis micro-accelerometers (Micro Strain 900/868 MHz G-link wireless; $\pm 2g$ range; 25 mm x 39 mm x 7.3 mm dimensions). Based on their draft, the initial buoy models had a natural heave frequency $\omega_{H0} \simeq 4.43$ r/s or $T_{H0} \simeq 1.42$ s, which corresponds to the prototype natural frequency, when applying a $\sqrt{\alpha}$ Froude scaling (e.g., White, 1999).

A first series of experiments were run that verified the near independence of the heave RAO, $Z_3(\omega)$, on D , in the period range $T = 0.5$ to 2.5 s. The independence of heave characteristics to buoy diameter was also verified by applying the numerical mod-

els, in both the standard WAMIT linear and the WM nonlinear, modes (the latter after calibrating the drag coefficient using experiments). Experiments also showed that parasitic roll oscillations were excited for $A > 0.03$ m in all the buoys, in part because of the proximity of the natural roll and heave periods for these buoys. Rolling led to increased viscous damping of the buoy heaving motion, which greatly reduced the heave RAO near resonance. Vertical fins were mounted on a buoy in order to limit roll oscillations, but this method met with limited success. A different system, made of multiple spar buoys, was developed to better separate the heave and roll natural frequencies, and reduce roll oscillations; this is detailed later.

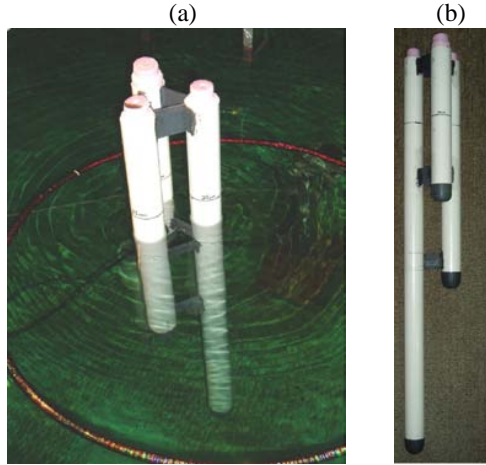


Fig. 2 : (a) Trispar buoy undergoing tests in the wave tank at resonant conditions (the vertical displacement of the spar far exceeds the amplitude of wave forcing); (b) Dry trispar.

A SSLG oscillators of mass 0.865 kg, including $M_s = 0.205$ kg for the spring and magnet mass, was built by TSI, and installed in a cylindrical casing of total length 0.99 m (Fig. 1b). A natural frequency $\omega_s = 4.49$ r/s ($T_s = 1.4$ s) was measured in both dry benchmark tests (Fig. 1b), and wavetank experiments of the generator. With this data, Eqs. (13) and (15) yield $l_s = 0.487$ m and $K_s = 4.13$ N/m. In the dry benchmark tests, the SSLG motion was forced in both amplitude (1.5 to 6 cm) and period (0.5 to 2 s), using a variable speed DC electric motor, and its power output was measured for one coil, using a rectifying circuit with varying resistance load. It was determined that, in the range of parameters tested, which simulates anticipated wave conditions in the tank, maximum power output (0.2-0.3 W for 1.5 cm amplitude at resonance period T_s) occurred for a 100 Ω load, the load that was later used in tank tests.

To accommodate the SSLG size, a longer and wider spar buoy than used before, referred to as SB3, was built with : $\ell = 1.28$ m, $D = 0.089$ m, $d = 1$ m, $M = 6.22$ kg (Fig. 1a). Due to its deeper draft, however, SB3 is resonant at $\omega_{H0} = 3.13$ r/s ($T_{H0} = 2$ s), which leads to a significant mismatch with both the target sea-state and ω_s and, hence, a low power generation with the SSLG.

In an effort to shift the heave resonance peak to lower periods, closer to T_s , and broaden the spectral response of the buoy (while reducing spurious roll oscillations, as mentioned before), we de-

signed and built a so-called “trispar” buoy model, made up of 3 spar buoys of diameter $D = 0.089$ m, draft $d = 0.25$ m, 0.50 m and 1.0 m, respectively, and total mass $M \simeq 10.89$ kg, mounted on an equilateral triangle arrangement (Fig. 2). To minimize the interference of the heave flow around each spar and keep the separation length of individual spars small compared to the forcing wavelength, the separation of the spars was set to D . The longer buoy in the trispar is identical to SB3 and can accommodate an internal SSLG. Each of the three spars has a different heave natural period ($T_{H0} = 1$ s, 1.4 s, and 2 s), covering the range of wave forcing in the tank. We will show that the trispar resonance period occurs near the average of the three buoys’, at $T_{H0} \simeq 1.6$ s, which is much closer to both T_s and the targeted T_p . Hence, as expected, we shall see that both the trispar heave RAO and SSLG power generation are greatly improved, as compared to SB3.

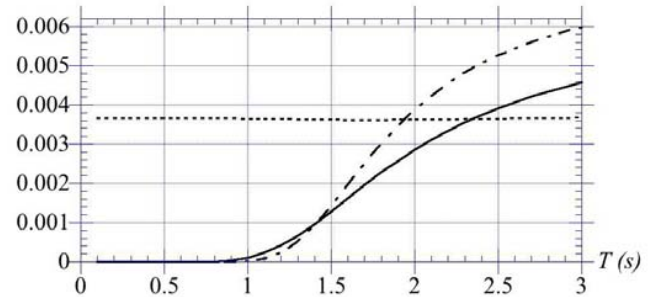


Fig. 3 : WAMIT results for SB3 buoy : (—) r'_3 ; (- - -) $20 a'_{33}$; (- · -) $1000 b'_{22}$.

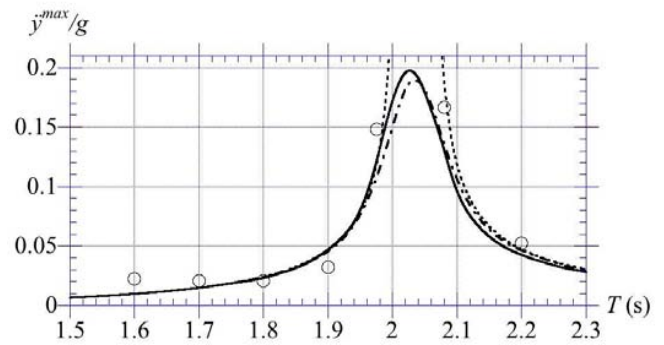


Fig. 4 : Maximum dimensionless heave acceleration for SB3, with $A = 0.015$ m: experiments (\circ); uncoupled WM results with $C_d = 0.4$ (- - -); coupled WM results with $C_d = 0.60$ (—); linear solution $-\omega^2 A Z_3$, from Eq. (10) (- · -).

The power production of various energy systems can be compared by calculating their Capture Width Ratio (Hagerman and Bedard, 2003), defined for a width W of the system, as $CWR = \overline{P}_\mu / (W P_w)$ with, for a periodic waves,

$$P_w = \frac{1}{2} \rho g A^2 c_g \quad ; \quad c_g = \frac{c}{2} \left\{ 1 + \frac{2kh}{\sinh 2kh} \right\} \quad (16)$$

the period-averaged power (in W/m) and group velocity, respectively ($c = \omega/k$ the phase velocity, with k given by Eq. (8) as a function of h and ω) and \overline{P}_μ the time-averaged output power (equal to $P_\mu^{max} / 2$ for a harmonic spring motion).

Details of experiments and WM simulations for SB3 and the trispar buoys are given in the following.

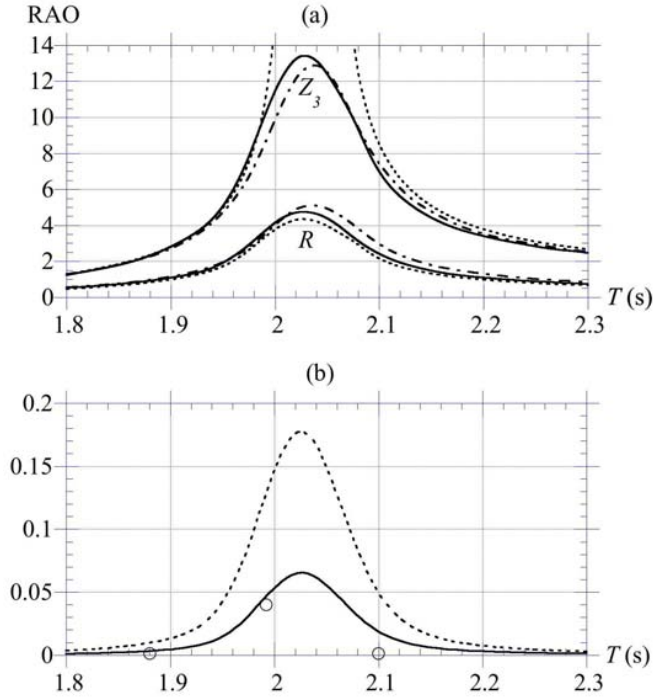


Fig. 5 : Simulation of SB3-SSLG system response (Figs. 3, 4 case). (a) Heave (Z_3) and spring (R) RAOs: coupled (—), uncoupled model (---); linear solution (---) (Eqs. (10) and (14)). (b) P_{μ}^{max} for $\mu' = 2.0$ in : experiments (\circ) (W); coupled WM simulations (—) (W); as the CWR for the latter (---).

Spar Buoy SB3 with SSLG in periodic waves

Buoy SB3, equipped with the SSLG system, was tested in the wavetank, for periodic waves of amplitudes $A = 0.015$ to 0.06 m, and depth $h = 1.3$ m (Fig. 1). In each case, both buoy heave acceleration and SSLG power output were measured, together with forcing wave characteristics. To compare measurements with simulations, WAMIT was first run for many periods (typically > 30), equally spaced between $T = 0.1$ and 3 s. Figure 3 shows the calculated dimensionless heave, added mass $a'_{33} = a_{33}/\rho$, radiative damping $b'_{33} = b_{33}/(\rho\omega)$, and wave forcing module $r'_3 = r_3/(\rho g)$. For all periods, $a'_{33} \simeq 0.00018$ ($\simeq 3\%$ of M) while $b'_{33} < 6 \cdot 10^{-6}$, hence confirming that, for a slender spar buoy, $\mathcal{K}(t) \simeq 0$ in Eqs. (1) and (3). We also see that very little wave forcing occurs for $T < 1$ s.

Fig. 4 compares maximum heave accelerations measured for SB3, as a function of wave period for $A = 0.015$ m, to those simulated with the WM model, using parameter values shown in Fig. 3. When running the model in uncoupled mode (i.e., neglecting the bracketed feedback force from the SSLG onto the buoy in Eq. (6)), a good fit is obtained between simulations and experiments by setting the drag coefficient to $C_d = 0.4$, which is a surprisingly low value, despite the likely turbulent conditions for the heaving flow. Heave resonance occurs in these simula-

tions for $T_H = 2.03$ s. When running the model in coupled mode, the buoy motion is slightly amplified near resonance by the SSLG oscillations and a good fit is obtained by using a larger value of $C_d = 0.6$. This value is more consistent with earlier tests of SB3 without the SSLG (not shown here), for which we found $C_d = 0.65$, and with the literature. [The Reynolds number based on buoy draft would be about 6.7×10^5 near resonance, which is in the turbulent regime. Experiments performed for buoys with smaller draft (and diameters) led to larger C_d values, which is consistent with the corresponding decrease in Reynolds number (e.g., White, 1999).] Heave resonance occurs in the coupled simulations for a slightly lower $T_H = 2.02$ s, which is close to $T_{H0} = 2$ s. The simulated values of maximum buoy acceleration (both uncoupled and coupled) agree very well with the linear analytic solution from Eq. (10), outside of a narrow period range $T = 1.95$ to 2.15 s, near T_H . This confirms that nonlinear viscous damping is negligible for small buoy motion but is dominant near resonance.

Fig. 5a shows the buoy heave RAO (Z_3) and corresponding spring-magnet RAO (R), predicted in the WM simulations, both uncoupled and coupled, as a function of the forcing period (case of Fig. 4). Different values of the damping parameter $\mu' = 0.5$ to 4 were tested and, as expected, the SSLG response greatly decreased with μ' . Fig. 5a shows results for $\mu' = 2$, which gives a reasonable fit for the predicted maximum power output of the SSLG in Fig. 5b, and compares these to the linear analytic solution, for Z_3 , Eq. (10) (note, the buoy heaving motion is only affected by that of the SSLG in the coupled simulations), and that based on the predicted maximum buoy acceleration, for R (i.e., applying Eq. (14) with $a_o = \dot{y}^{max}(\omega)/A$ in the coupled WM model). We see that the nonlinear and linear results agree very well for Z_3 , outside of the resonant period range mentioned earlier and, as expected, for R , both coupled WM and corresponding linear results agree very well for all periods, since the SSLG is a linear oscillator. The maximum magnet motion amplitude at resonance is $z^{max} \simeq 4.7A$, or 7 cm, while the maximum heave amplitude is $y^{max} = 13.5A$ or 0.2 m.

Fig. 5b shows coupled simulations of the maximum power generated by the SSLG, as a function of the forcing period, for $\mu' = 2$. A few maximum output powers, measured in laboratory tests with the 100Ω circuit, are also shown on the figure. We see, the selected μ' value gives a reasonable fit of these to simulations. Maximum predicted power at resonance is a modest 0.07 W. Finally, Fig. 5b shows the CWR, defined in Eq. (16), simulated as a function of wave period for $W = D$. A maximum value of 18% is reached at resonance, but the CWR becomes less than 5% , outside of a 0.14 s wide period range from $T = 1.96$ - 2.1 s. Hence, the SB3-SSLG system is moderately efficient at capturing energy from periodic waves very near its natural heave period.

Trispar Buoy with SSLG in periodic waves

The trispar buoy, equipped with a SSLG in its longer buoy, was similarly tested and simulated in periodic waves. WAMIT was first run for the trispar geometry, to calculate added mass, damping, and forcing parameters (Fig. 6). Fig. 6a shows the trispar added mass, compared to that of SB3. We see that a'_{33} is

shifted to lower periods for the trispar and represents about 5% of its mass. Applying Eq. (11) with this data yields a lower natural heave period for the trispar than for SB3, $T_H = 1.57$ s, which is now close to both T_s and T_p . In Fig. 6b, the wave forcing term is also shifted to lower periods, and is uniformly larger than for SB3, implying that the trispar buoy will have a better response to smaller period waves near the targeted sea-state period than SB3. Note, $r'_{3L} = (S_o / \cosh kh) \sum_{i=1}^3 \cosh k(h - d_i)$, the pressure force acting on the trispar buoy based on the undisturbed incident wave (i.e., neglecting diffraction), is marked on the figure; we see, r'_{3L} is 15% to 20% higher than the actual force r'_3 , from $T = 1$ to 2 s, consistent with increased diffraction effects as kD increases (i.e., towards lower wave periods). Data in Fig. 6 was used in Eq. (7), together with $c_{33} = 3\rho g S_o$, $b = 3\rho S_o C_d/2$, and $d = 0.5$ (corresponding to the trispar mean draft), to perform coupled WM simulations of the trispar-SSLG system.

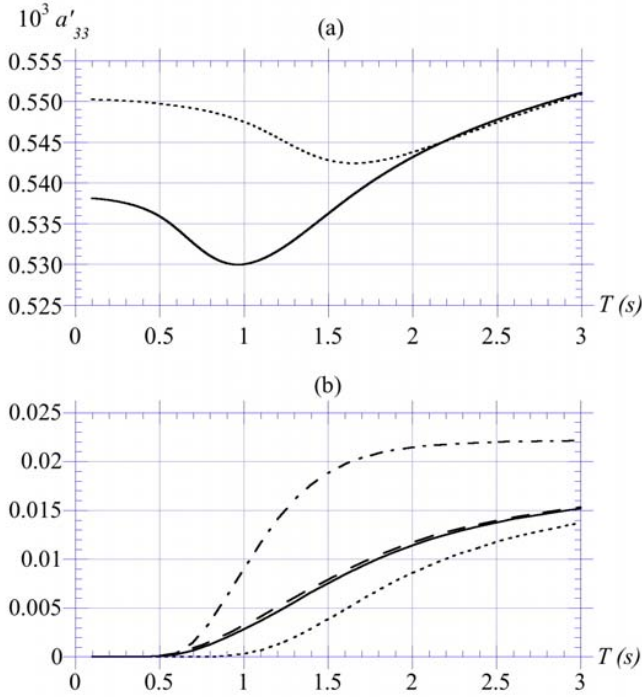


Fig. 6 : WAMIT trispar parameters: (a) a'_{33} (—), $3 a'_{33}$ (SB3) (- -); (b) r'_3 (—), r'_{3L} (— —), $1000 b'_{33}$ (— · —), $3 r'_3$ (SB3) (· · ·).

Fig. 7a shows results for the trispar maximum dimensionless heave acceleration, for $A = 0.015$ m. The nonlinear results agree quite well with laboratory experiments when specifying $C_d = 0.4$. This drag coefficient value, much smaller than for SB3 (0.6), in fact, is a non-physical average for the 3 spar buoys in the trispar. The trispar drag force in Eq. (6) is indeed defined using a w value corresponding to the average draft, which leads to larger relative velocities $|\dot{y} - w|$ for the shallower draft buoy than actually experienced and, hence, an artificially low overall C_d (although clearly more experiments should have been performed near the resonance peak in order to better calibrate C_d). As expected, maximum heave amplification occurs for $T = T_H = 1.57$ s, with acceleration $\ddot{y}^{max} \simeq 0.28 g$, corresponding to RAOs (both not

shown) $Z_3 = 11.3$, slightly smaller than for SB3, and $R = 7.0$, much larger than for SB3 because of the proximity of T_s and T_{H0} . As for SB3, the linear results derived from Eq. (10) for the heave acceleration, agree very well with the nonlinear results, outside of a narrow resonance band, from $T = 1.52$ to 1.68 s, where nonlinear viscous drag becomes large.

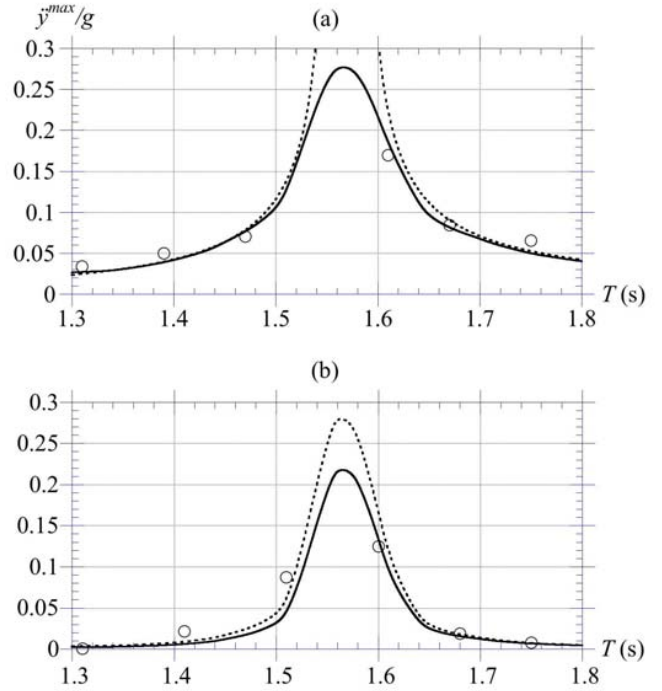


Fig. 7 : Trispar-SSLG response for $A = 0.015$ m (Fig. 2). (a) Maximum heave acceleration: experiments (o); coupled simulations for $C_d = 0.4$ (—); linear solution (- - -). (b) Maximum power P_{μ}^{max} generated by the SSLG: in experiments (o) (W); in coupled simulations for $\mu' = 1.5$ (—) (W); as the CWR (- - -).

Fig. 7b shows the maximum output power simulated for the buoy motion shown in Fig. 7a, using a damping coefficient $\mu' = 1.5$. With this value, simulations agree well with most laboratory measurements (although, again, more measurements should be made near the resonance period in order to make a better comparison and calibrate this coefficient). The maximum output power predicted at resonance is $P_{\mu}^{max} = 0.22$ W. This would correspond to 696 W at prototype scale for the target sea-state, with $T_p = 4.5$ s and wave height $H = 0.3$ m (scaling with $\alpha^{3.5}$). For sinusoidal motion, the mean output power at prototype scale would thus be 348 W. The figure also shows the simulated CWR (using $W = 3D$), which reaches a maximum value of 28% at resonance, becoming less than 5% outside of a 0.13 s wide period range, from $T = 1.51$ to 1.64 s.

Simulations in irregular waves

Realistic sea-states can be simulated using a PM or JS spectrum as input, and performing WM simulations, using parameters calculated with WAMIT as detailed before. To interpret results, we define Root Mean Square (rms) values of parameters such as

y , \ddot{y} , and a time-average for P_μ . Working at laboratory scale, we specify a significant wave amplitude for a JS spectrum (with peakedness $\gamma = 3.3$), corresponding to the same incident P_w as for periodic waves used earlier, i.e., $A_s = 0.015\sqrt{2} = 0.021$ m. For a given spectral peak period T_p , fetch F and wind speed at 10 m, U_{10} are then iteratively calculated. Table 1 shows results of simulations, up to $t = 150 T_p$, of the trispar-SSLG response to such sea-states, with $C_d = 0.4$ and $\mu' = 1.5$ (calibrated earlier). Near $T_H = 1.57$ s, we find $\overline{P_\mu} \simeq 0.09$ W and a good $CWR = 16\%$. Table 1 shows, $\overline{P_\mu}$ stays within 50% of its peak value for $1.3 < T_p < 2.2$ s, which is a wider period range of performance (0.9 s) than for periodic wave forcing (0.65 s).

T_p (s)	F (km)	U_{10} (m/s)	$\text{rms}(\frac{y}{A_s})$	$\text{rms}(\ddot{y})$ (m/s ²)	$\overline{P_\mu}$ (W)	CWR (%)
1.20	0.28	25.4	2.22	0.77	0.026	6.5
1.30	0.42	21.9	2.75	0.94	0.038	8.8
1.40	0.58	19.5	3.37	1.16	0.055	12.2
1.50	0.81	17.2	4.18	1.40	0.081	16.2
1.57	1.0	16.0	4.34	1.45	0.088	16.2
1.60	1.1	15.4	4.50	1.47	0.088	16.2
1.70	1.5	13.8	4.01	1.33	0.074	12.0
1.80	1.9	12.5	3.86	1.26	0.067	10.1
1.90	2.5	11.5	3.68	1.21	0.059	8.7
2.00	3.1	10.7	3.34	1.13	0.052	7.1
2.10	3.9	9.80	3.26	1.09	0.048	6.2
2.20	4.9	9.00	3.15	1.04	0.044	5.3

Table 1 : Irregular wave Trispar-SSLG simulations (JS, $\gamma = 3.3$, $A_s = 0.021$ m, $C_d = 0.4$, $d = 0.5$, $\mu' = 1.5$, $T_s = 1.4$ s).

CONCLUSIONS

We studied the performance of a trispar-SSLG system, that we propose as a low power source for marine surveillance systems, based on renewable wave energy. The trispar-SSLG system is much more efficient at capturing energy from small amplitude periodic waves than a single spar (SB3), although optimal performance still occurs within a narrow period band near the natural heave period. Unlike SB3, the trispar does not experience spurious roll oscillations for larger wave amplitudes. We find a factor of 3.5 gain in power production by the trispar vs. SB3, under the same small amplitude wave forcing ($A = 0.015$ m), for both the measured and simulated power. The CWR for the trispar is more than 50% greater than for the single spar. [Note, using $W = \sqrt[3]{\overline{y}/\rho}$ in the definition of CWR , as is being suggested in the community, would further increase the relative performance of the trispar vs. SB3 by a factor of 2.5.] Preliminary simulations of the trispar under irregular wave forcing also yield promising power output and CWR values. These findings give us a strong incentive for further pursuing the trispar design.

Let us finally recall that μ' should not be a constant in the model, but depend on the electro-magnetic interactions between the spring-magnet system circuit and the magnet motion, itself frequency dependent. More work is clearly needed in this respect. Also, this study was restricted to fixed tuning strategies; we are planning in future work, to explore slow and fast tuning,

strategies, or more sophisticated control of the generator. As an example, recent work by Babarit et al (2006), based on original ideas proposed by Budal and Falnes (1980), shows that latching control of wave energy systems can dramatically increase the bandwidth of response of the system, particularly at sub-resonant periods, and hence power production. Latching control of the present wave energy device would consist of locking the SSLG magnet in position, at the instant when its velocity is zero, and releasing it after some time lag in order to put its velocity (as much as possible) in phase with wave forcing, thus maximizing its velocity and power generation.

REFERENCES

- Babarit, A., and A. H. Clément, (2006) "Optimal latching control of a wave energy device in regular and irregular waves," *Applied Ocean Res.*, **28**, 77-91.
- Baker, N.J. and M.A. Meuller (2004). "High and low density linear electric machines for marine renewable energy converters," *IMarEST Marine Renewables Energy Conf.* (MAREC, Blyth, UK, July 2004).
- Baker, N.J., M.A. Meuller, P.J. Yavner, and L. Ran (2005) "Prototype development of a direct drive linear electrical machines for marine energy converters," *World Renewable Energy Congress IX* (WREC 2005), Elsevier Ltd.
- Berteaux, H.O, (1994) *Coastal and oceanographic buoy engineering*, H.O. Berteaux, Woods Hole, MA, 285pps.
- Budal, K. and J. Falnes (1975) "A resonant point absorber of ocean wave power," *Nature*, **256**, 478-479.
- Budal, K. and J. Falnes (1980) "Interacting point absorbers with controlled motion," in *Power from Sea Waves*. BM Count, Academic Press.
- French, M. J. (1979) "A generalized view of resonant energy transfer," *J. Mech. Engng. Science*, **21**, 299-300.
- French, M. J. and R. H. Bracewell (1995) "The systematic design of economic wave energy converters," *Proc. ISOPE95 Conf.* (The Hague, Netherlands, June 11-16).
- Hagerman, G. and R. Bedard (2003) "Guidelines for preliminary estimation of power production, by offshore wave energy conversion devices," EPRI Rpt. 297213.
- Lee, C.-H. (1995) *WAMIT Theory Manual*. MIT Report 95-2, Dept. of Ocean Eng., MIT.
- Newman, J., (1977). *Marine Hydrodynamics*, MIT Press Cambridge, MA (9th reprint).
- Previsic, M., R. Bedard, and G. Hagerman (2004). "Assessment offshore wave energy conversion devices," Report No: E21 EPRI. WP-004-US-Rev 1. June 16, 2004
- Stallard, T., R. Rothschild, A. Bradshaw, and G. Aggidis (2005) "Comparison of equivalent capacity wave energy schemes," *Proc. World Renewable Energy Congress IX* (WREC 2005).
- White, F.M. (1999) *Fluid Mechanics*, WCB McGraw-Hill, Boston, MA, 826 pps. (4th edition).

ACKNOWLEDGEMENTS

This research was supported by Teledyne Scientific & Imaging, LLC, as part of a US DARPA grant. S. Leblanc (LSEET, Univ. of Toulon, France) is acknowledged for fruitful discussions.